

Electron Cloud Simulations for the Electron-Ion Collider in Brookhaven National Laboratory

X. Gu

November 2022

Electron-Ion Collider
Brookhaven National Laboratory

U.S. Department of Energy

USDOE Office of Science (SC), Nuclear Physics (NP) (SC-26)

Notice: This technical note has been authored by employees of Brookhaven Science Associates, LLC under Contract No. DE-SC0012704 with the U.S. Department of Energy. The publisher by accepting the technical note for publication acknowledges that the United States Government retains a non-exclusive, paid-up, irrevocable, world-wide license to publish or reproduce the published form of this technical note, or allow others to do so, for United States Government purposes.

DISCLAIMER

This report was prepared as an account of work sponsored by an agency of the United States Government. Neither the United States Government nor any agency thereof, nor any of their employees, nor any of their contractors, subcontractors, or their employees, makes any warranty, express or implied, or assumes any legal liability or responsibility for the accuracy, completeness, or any third party's use or the results of such use of any information, apparatus, product, or process disclosed, or represents that its use would not infringe privately owned rights. Reference herein to any specific commercial product, process, or service by trade name, trademark, manufacturer, or otherwise, does not necessarily constitute or imply its endorsement, recommendation, or favoring by the United States Government or any agency thereof or its contractors or subcontractors. The views and opinions of authors expressed herein do not necessarily state or reflect those of the United States Government or any agency thereof.

Electron Cloud Simulations for the Electron-Ion Collider in Brookhaven National Laboratory

Xiaofeng Gu, Alexei Blednykh, Michael Blaskiewicz,
Guillaume Robert-Demolaize, Silvia Verdú-Andrés

November 30, 2022

1. Introduction

For high-intensity circular accelerators and storage rings, if the secondary electron emission yield (SEY) of the vacuum chamber surfaces is high, an EC (Electron Cloud) could build up with the passage of the circulating beam [1] [2] [3] [4] [5] [6] [7]. The presence of EC can strongly affect the beam quality, such as transverse instabilities, transverse emittance growth, and beam loss. Furthermore, the heat load from EC can exceed the available cryogenic capability. For the RHIC superconducting (SC) arc magnets, to be used for the hadron storage ring of the Electron-Ion Collider (EIC), the dynamic heat load budget is 0.5 W/m to the 4.5 K stainless steel beam pipe [8]. This can limit the maximum beam bunches or intensity of the EIC, hence diminishing the luminosity provided by the EIC.

The EC has affected the beam instability and significantly contributed to cryogenic heat load in the Large Hadron Collider (LHC) [1] [2] [3]. Positron storage rings for which ECs have been a critical factor in the design and performance include KEKB in Japan [4] [5] and EC buildup remains one of the concerns for future high-intensity accelerators design. EC considerations have driven the SuperKEKB collider design [6] and the positron damping ring for the proposed International Linear Collider (ILC) [7]. The LHC luminosity upgrade is contingent on reducing the bunch spacing to 25 ns [9]; at this bunch spacing, severe EC buildup has been observed [5]. The success of the upgrade is likely contingent on limiting EC buildup.

To study the EC heat load, we did some EC simulations with PyECLLOUD code [9] for the dipole, quadrupole, sextupole magnets, and the warm (drift) section of the EIC hadron storage ring. PyECLLOUD is an EC simulation code developed by CERN. The code has been validated and used to study EC in the LHC, SPS, and PS.

To eliminate EC buildup, the sources of electrons must be minimized. First, we will reduce the production of electrons due to residual gas ionization by specifying the maximum gas density, which requires a vacuum chamber with low electron-stimulated desorption (ESD) yields and a sufficient (preferably distributed) pumping speed. Second, we should reduce the secondary electrons with a lower secondary electron yield (SEY) material.

2. The secondary electron emission model

The SEY and its model are the most critical parameters for the EC simulation. There are two SEY models used in the PyECLLOUD code. The first model is called 'ECLLOUD model' which is inherited from the ECLLOUD code [10]. Another model in PyECLLOUD code is the so-called 'Furman and Pivi' Model [11] [12], which is also used in other simulation codes like POSINST and open-Ecloud.

The ECLLOUD model in the PyECLLOUD code is based on laboratory mea-

measurements performed on a copper surface [10], while the FP model is evaluated via copper as well as stainless steel Montcarol simulation data [11]. If possible, the measured SEY for relevant materials should be checked against different SEY models before EC simulation studies.

The secondary electron emission yield (SEY or δ) is defined as the ratio between the emitted secondary electron current and the incident electron current:

$$\delta(E_0, \theta_0) = \frac{I_{emitted}}{I_{incident}} \quad (1)$$

where E_0 and θ_0 are the energy and angle of the incident electrons.

The two different SEY models have different dependence of δ on E_0 , θ_0 , the emitted electron energy, and angle distribution.

In the ECLLOUD model, the total SEY can be expressed as the sum of two components, the true secondary electrons, and the elastically reflected electrons.

$$\delta(E_0, \theta_0) = \delta_{elas}(E_0) + \delta_{true}(E_0, \theta_0) \quad (2)$$

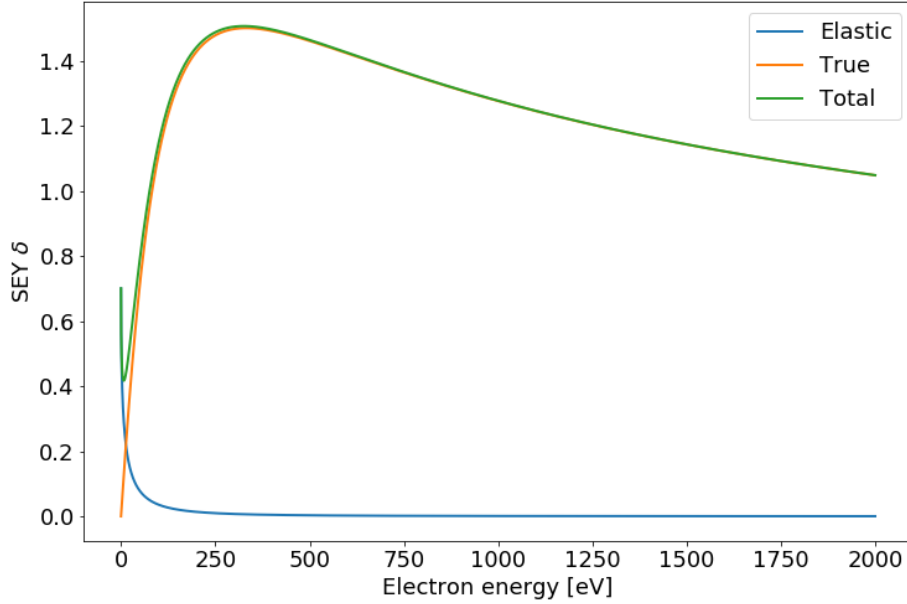


Fig. 1: The SEY of ECLLOUD model as a function of electron energy.

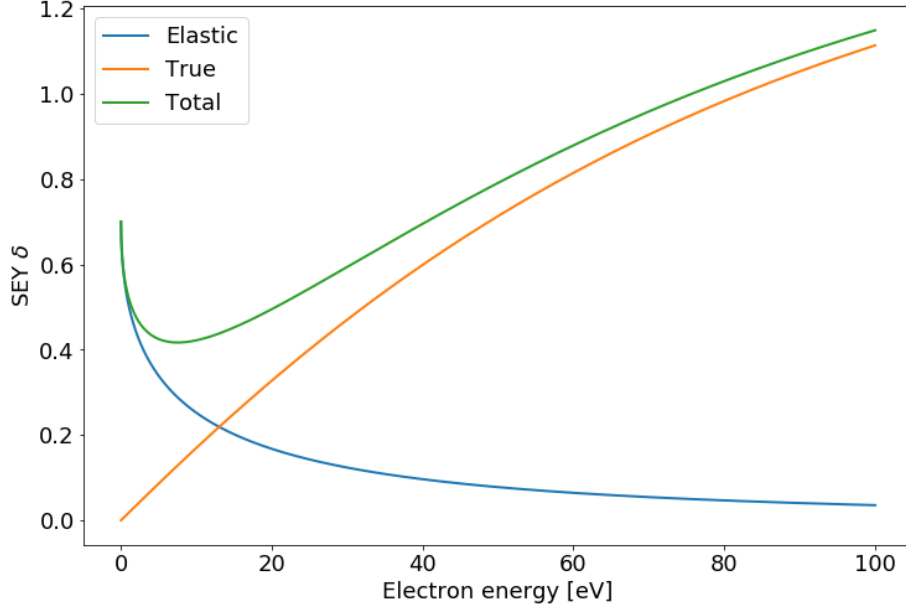


Fig. 2: The SEY of ECLLOUD model as a function of electron energy for low electron energy region.

The two components are defined below [10] [13]:

$$\delta_{elas}(E_0) = R_0 \left(\frac{\sqrt{E_0} - \sqrt{E_0 + E_e}}{\sqrt{E_0} + \sqrt{E_0 + E_e}} \right)^2 \quad (3)$$

$$\delta_{true}(E_0, \theta_0) = \delta_{max}(\theta_0) \frac{s \frac{E_0}{E_{max}(\theta_0)}}{s - 1 + \left(\frac{E_0}{E_{max}(\theta_0)} \right)^s} \quad (4)$$

where the SEY and energy dependence on the angle of incidence are defined as:

$$\delta_{max}(\theta_0) = \delta_{max} e^{(1 - \cos \theta_0)/2} \quad (5)$$

$$E_{max}(\theta_0) = E_{max} [1 + 0.7(1 - \cos \theta_0)] \quad (6)$$

where δ_{max} and E_{max} are the maximum point of the SEY curve and its corresponding energy for $\theta_0 = 0$. E_e and s are the shape parameters of the reflected SEY curve and the true SEY curve, respectively; R_0 is the weight of the reflected electron component. The SEY curves of the ECLLOUD model are plotted in Fig. 1 and Fig. 2, and the angular dependence is illustrated in Fig. 3.

For the energy and angle distribution in ECLLOUD model, the elastic reflected electrons have the same energy and opposite angle as the incident electrons. The energy distribution or energy spectrum of the true emitted secondary electron is

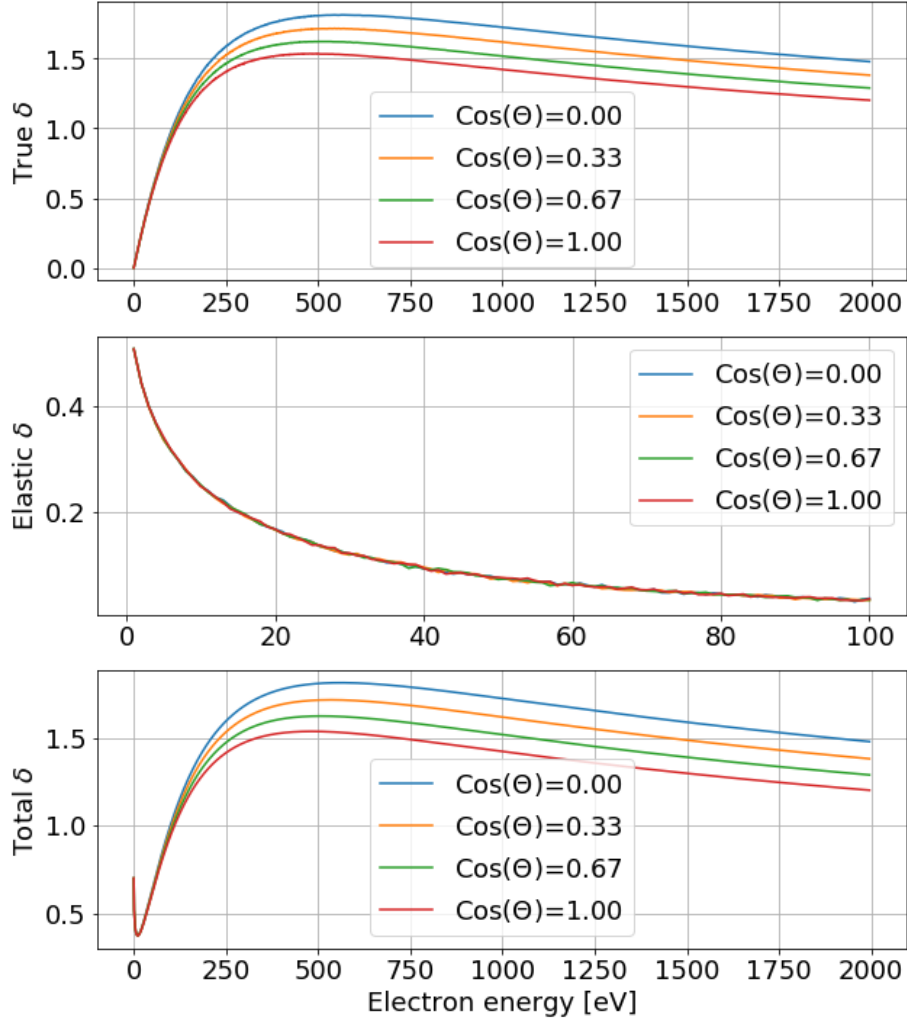


Fig. 3: The SEY of ECLLOUD model and incident angle. The angle is measured relative to the normal surface. Both E_{max} and δ_{max} increase as the angle increases

fitted by a ‘lognormal’ distribution in the form:

$$\frac{dn_{true}}{dE} = \frac{1}{\sqrt{2\pi}E_0\sigma_{true}} e^{-\frac{[\ln(E_0) - \mu_{true}]^2}{2\sigma_{true}^2}} \quad (7)$$

where $\mu_{true} = 1.6636$ and $\sigma_{true} = 1.0826$ are the two fitting parameters of the log-normal energy distribution in the model. Fig. 4 shows the energy spectrum of the emitted true secondary electrons.

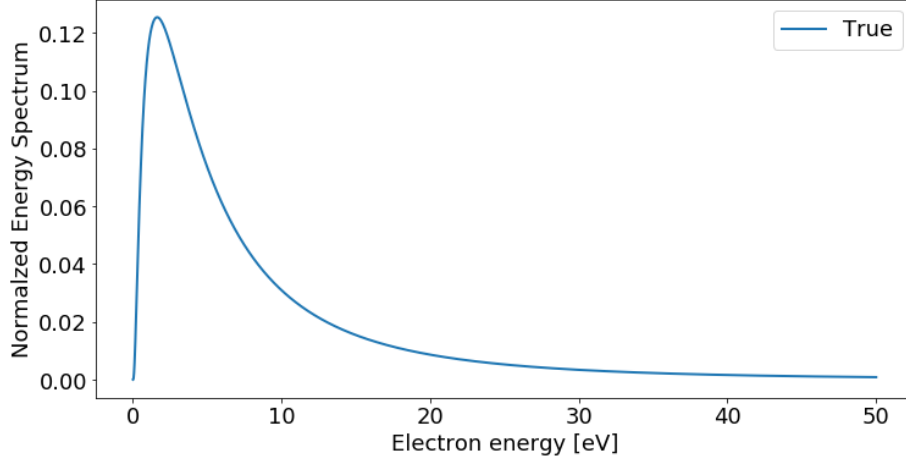


Fig. 4: The true secondary electron spectrum of the ECLLOUD model. The elastic electrons have the same energy as the incident electrons, no plot is provided.

The angle of incidence of the incident electron is also included in the model. The angular distribution of the true secondary electron in PyECLLOUD is named ‘cosine 2D’ or ‘cosine 3D’ for the 2D or 3D case. They can be expressed as:

$$\frac{dn}{d\theta} = \cos \theta \quad (8)$$

$$\frac{dn}{d\theta} = \cos \theta \sin \theta \quad (9)$$

The 3D cosine distribution is more accurate because it takes into account the surface element $\sin \theta$ in spherical coordinates [9]. Some SEY simulation parameters used in this paper are listed in Table 1. The Furman-Pivi Model is discussed in Appendix A.

Table 1: Secondary electron emission parameters for different materials used in our simulations.

Quantity	Unit	Scrubbed SS316L [19]	Copper	Amorphous carbon [22]
R_0		0.5	0.7	0.7-0.9
E_0	eV	225	150	150
E_{max}	eV	250	332	275.1
s		1.357	1.35	1.773
δ_{max}		1.48	1.1-1.7	1.06
σ_{true}	eV	1.0828	1.0828	1.0828
μ_{true}	eV	1.6636	1.6636	1.6636

3. EC Buildup

An EC could be built up with the following conditions and procedures. Firstly, the maximum SEY of the vacuum chamber should be higher than 1. Then, some electrons are generated via bunched beam-induced residual gas ionization or photoemission. After that, these electrons are accelerated up to several hundred eV by an electric field (perpendicular to the bunched beam) which is generated by the same bunched beam or the next bunched beam. They will hit on a vacuum wall and create some secondary electrons (usually less than 50 eV) which may travel back and forth or oscillate inside a vacuum chamber.

Some secondary electrons could be absorbed or elastically reflected by the vacuum wall, and the SEY for them is usually less than 1 because of their low energy (see Fig. 5). Therefore, the number of these secondary electrons will be less and less. Other secondary electrons could be accelerated up to several hundred eV again if they are very close to the center when the next bunched beam comes. This is the reason that an EC could be built up.

According to the above discussion, the EC build-up is determined by the position of the secondary electron when the next bunched beam arrives. The longitudinal bunch space-time span is $t_{b\text{space}}$ for a bunched beam train. The transverse traversal time $t_{e\text{cloud}}$ of secondary electrons is the time cost of returning to the center after they leave the center and hitting the vacuum chamber. We assume that there is only one time to collide in the vacuum chamber before accelerating the next bunch arrives. The bunch intensity, bunch length, vacuum chamber size, and magnetic field [12] can affect the electron beam traversal time $t_{e\text{cloud}}$.

If $t_{b\text{space}} = kt_{e\text{cloud}}$ while k is an integer, a resonance condition could be established. With this resonance condition, when the next bunched beam comes, the overall electrons (which are dominated by less than 50 eV low-energy secondary electrons) travel very close to the bunched beam center and are

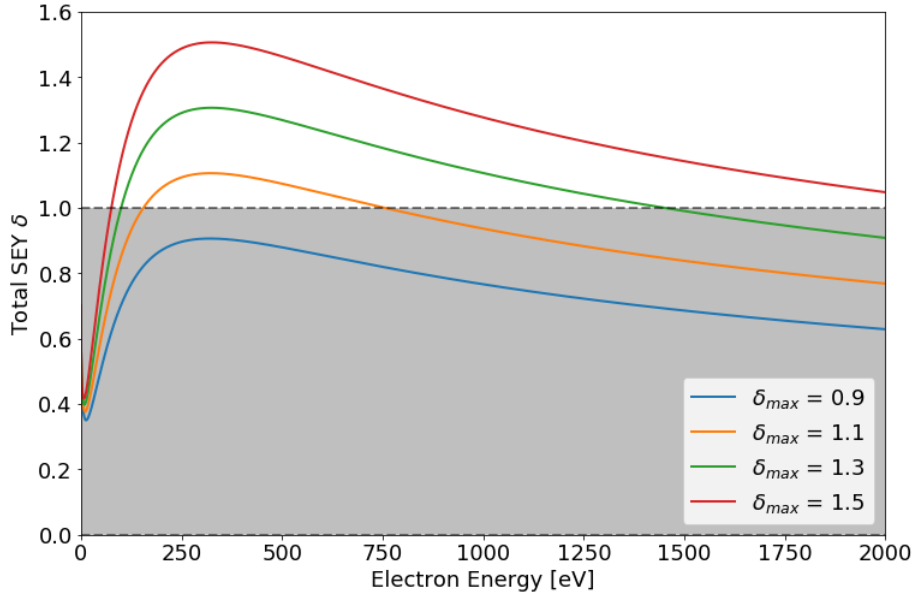


Fig. 5: The SEY plots with different δ_{max} . The gray area indicates the SEY is less than 1.

accelerated to higher energy again. With higher electron energy close to the δ_{max} , the SEY could be higher than 1 (Fig. 5).

The velocity or energy of the secondary electrons is different, not all electrons have the same traversal time t_{cloud} and could be a continuous time range. Therefore, if there are more electrons than the previous beam passage around the center, that is enough for an EC build-up.

On the other hand, when the next bunch comes, if the overall electrons are far from the center, they will be less affected by the bunched beam.

The electron density within the vacuum chamber for a bunched beam with 10 nS and 30 nS longitudinal bunch spacing are shown in Fig. 6 and Fig. 7, respectively, without and with resonance. There is no EC build-up if the electron density around the center of the beam orbit is small when the bunch arrives, as deduced from Fig. 6. There will be an e-could build-up when there are enough electrons along the beam orbit.

To verify the above explanation, we did some EC simulations with different longitudinal bunch spaces $t_{b\ space}$ for different magnet types. The heat load from the impacts of the EC is used to monitor the EC strength. From Fig. 8, the EC buildup starts from $t_{b\ space} = 17.5$ nS for both dipole and quadrupole. If the bunch spacing is less than 17.5 nS, the bunch arrives too early, and there are not enough electrons around the center to be accelerated again. Meanwhile, if the

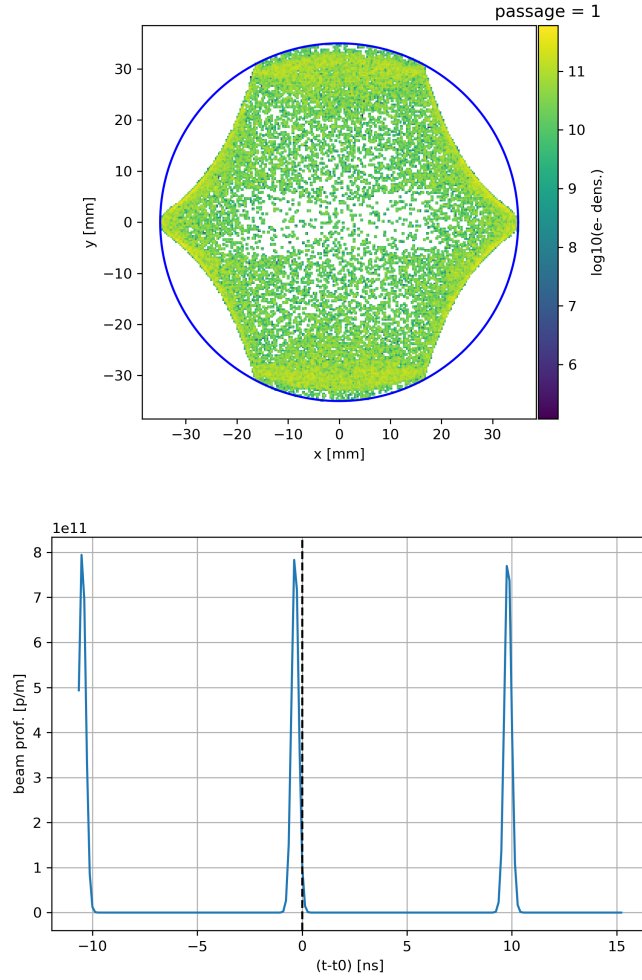


Fig. 6: Electron density for a bunched beam with 10 ns bunch spacing.

bunch space is too long (45 ns for quadrupole magnet), the secondary electron density around the center decay to a level that is less than the previous value when the bunched beam arrives. That means there is no electron build-up.

To evaluate the t_{ecloud} effects on the EC buildup resonance, we did some EC simulations now with a different beam pipe radius. Fig. 9 shows the heat load as a function of beam pipe radius for quadrupole magnets. For 10 ns longitudinal space-time and a vacuum chamber radius of less than 30 mm, the t_{ecloud} is short, and some secondary electrons reach the center while the next bunch arrives. With a larger beam pipe radius (30 mm-54 mm) and therefore a longer time to arrive at the center, the next bunch passes before the secondary electrons

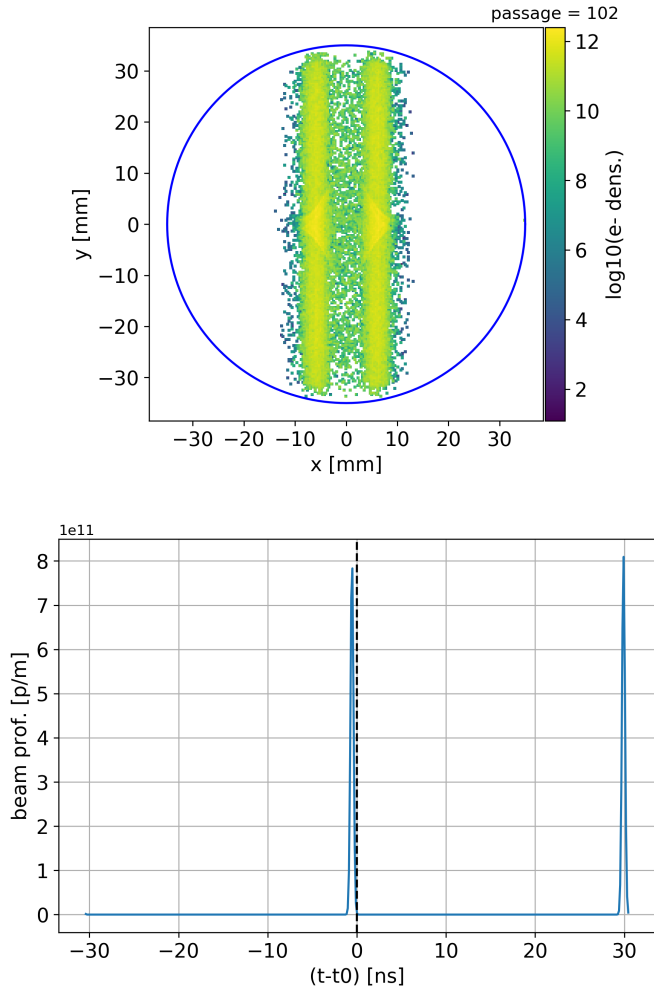


Fig. 7: Electron density for a bunched beam with 30 ns bunch spacing.

reach the center. With a radius greater than 58 mm, there is more time for the secondary electron beam to reach the center. We suspect that it is the second bunch that accelerates the electrons again.

For the 40 ns longitudinal space-time, with a beam pipe radius less than 24 mm, it is suspected that the t_{ecloud} is too short and the secondary electrons pass through the center again before the next bunch arrives. With 26 mm and 40 mm radii, the travel time of some secondary electrons is long enough to meet the next bunch around the center, and therefore there is EC buildup.

Fig. 10 shows the increased number of impacting electrons per unit of length at each bunch passage. More details about the EC buildup are found in Ref. [10].

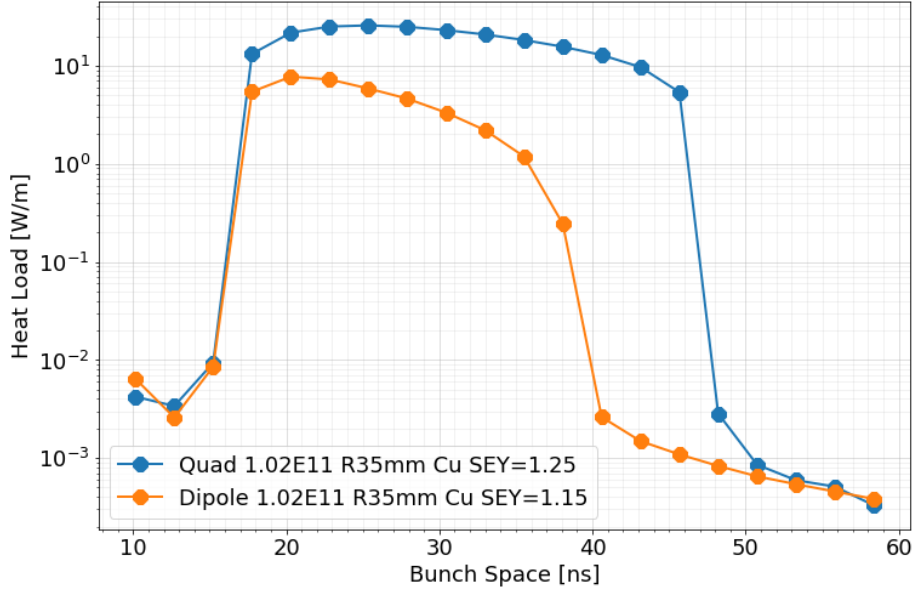


Fig. 8: Heat load with different bunch space-time $t_{b\text{space}}$. The surface of the 35 mm-radius beam pipe has a SEY of 1.15 and 1.25 and is embedded in a quadrupole field. The bunch intensity is $1.02e11$ protons per bunch.

The kinetic energy of secondary electrons is usually less than 50 eV. Therefore, the cyclotron radius of their trajectory in a magnetic field is less than several millimeters [10]. This implies that these secondary electrons move around and follow the magnetic field line. If the magnetic field has a transverse or longitudinal gradient, it can form a magnetic bottle or mirror [16]. The magnetic field bottle effect may also play an important role via trapping more electrons and enhancing the EC [10]. Fig. 11 shows the typical electron density pattern in quadrupole and sextupole magnets for a beam passing through the center of a round pipe.

The number of 'seed' of initial electrons is, for the 275 GeV proton beam circulating in the EIC hadron storage ring, dominated by the residual gas. Electron photoemission due to synchrotron radiation is negligible.

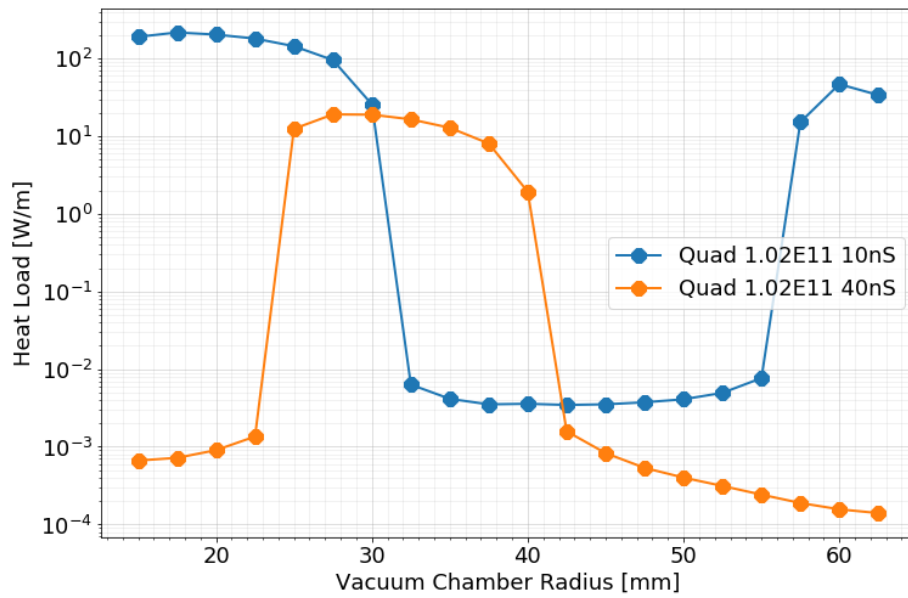


Fig. 9: The heat load with different vacuum pipe radius.

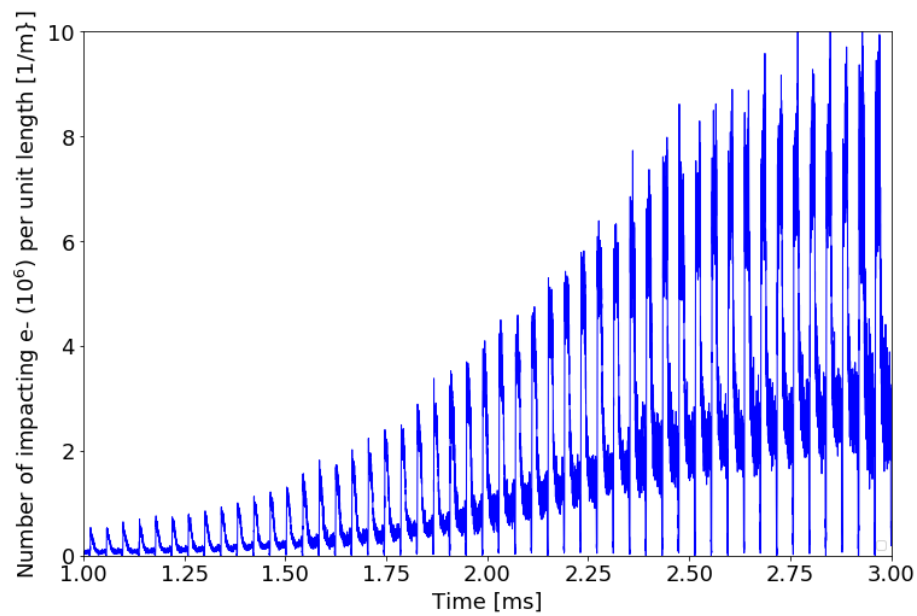


Fig. 10: The plot shows the number of impacting electrons per unit for each bunched beam passage.

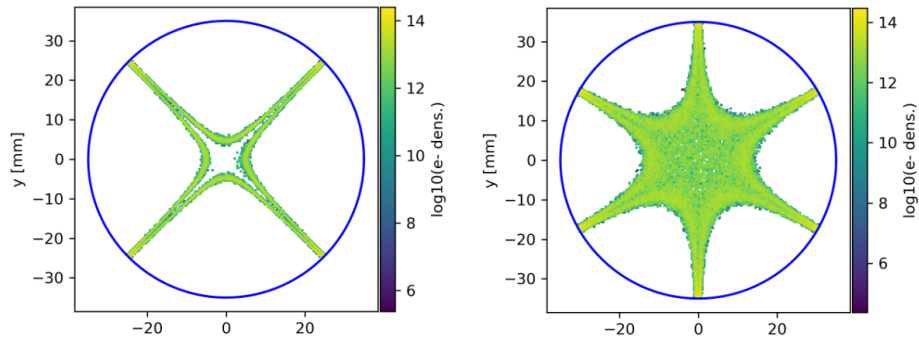


Fig. 11: Electron density in quadrupole and sextupole magnet.

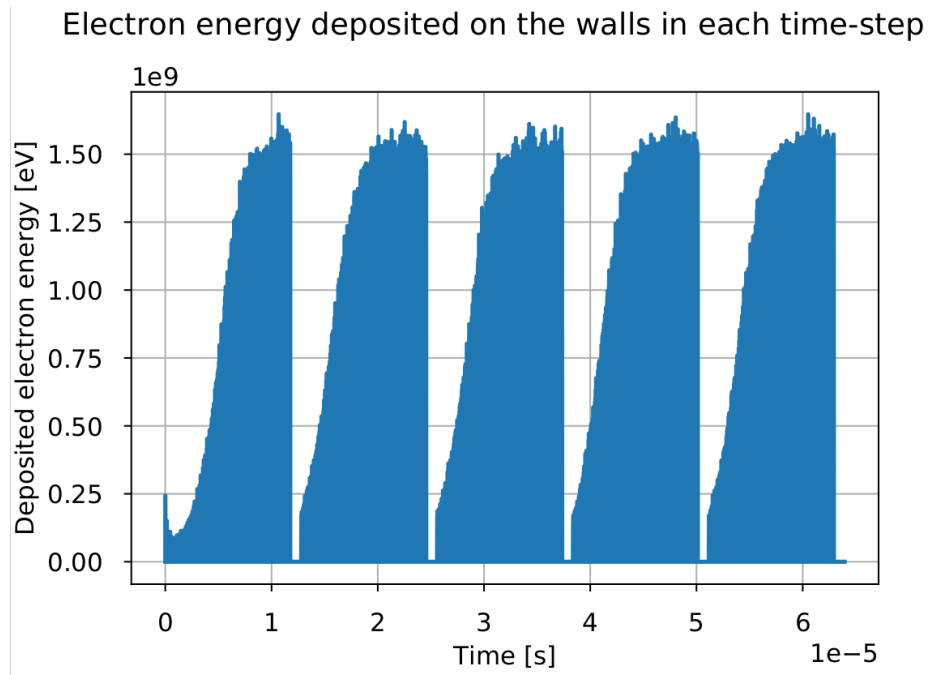


Fig. 12: EC Buildup with 5 turns

4. EC buildup thresholds in the EIC hadron storage ring

4.1. Simulation setup and parameter evaluation

The PyECLOUD code has four input files. The beam parameter file includes the beam size, emittance, bunch space, bunch intensity, bunch length, filling pattern, etc. The machine parameter file has the parameters about vacuum chamber size, magnetic field, etc. The secondary emission file contains the material's SEY

parameters. The simulation parameter file is about the EC buildup simulation settings.

In an EC buildup simulation, the number of turns or total bunch passages may affect the number of secondary electrons, and thus the heat load from EC, if the EC survives the abort gap. Fig. 12 shows a five-turn EC buildup progress. For the first turns, the EC buildup is slower than for the other four turns. Therefore, the heat load will be less than the average of many turns or the average of the other four turns if there is only one turn simulation. This is important if the EC buildup is slow. Within this note, we did all simulations with 5 turns.

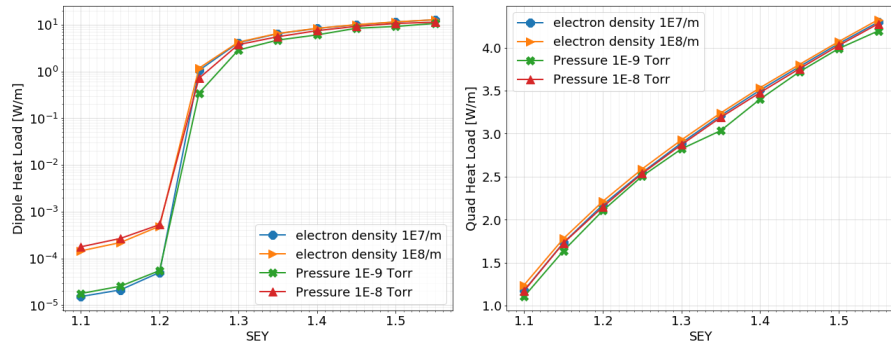


Fig. 13: EC build-up in dipole and quadrupole magnet with different initial electron density and pressure.

The seed or initial electrons could be provided as a uniform initial electron density or generated by ionization. To evaluate the effects of the initial number of electrons, the heat load with different initial conditions is computed and shown in Fig. 13 for the high luminosity beam of the EIC (with 1160 bunches or 10 ns bunch spacing) and for the RHIC arc dipole and quadrupole magnets. There is no significant difference between different initial conditions when there is EC buildup.

Simulation step time is another parameter that may affect the EC buildup simulation result. The variation of the heat load computed for various simulation time steps is shown in Fig. 14. The reason for the quadrupole heat load oscillation with different step times still needs further study. But it won't affect the conclusions in this note. We care more about whether there is an e-cloud buildup or not, rather than an absolute value. Finally, a time step of 10 ps is used for all the below simulations.

4.2. RHIC SC arc magnets with stainless steel beam pipe

To evaluate whether the RHIC existing 70 mm-diameter radius stainless steel beam pipe requires any coating to suppress EC buildup or not, some EC buildup

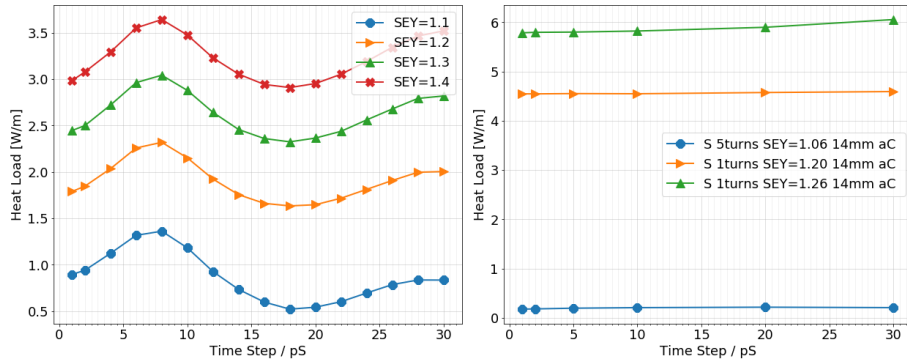


Fig. 14: EC buildup simulation in quadrupole magnet (left) and sextupole magnet (right) with different simulation time steps.

simulations for the dipole and quadrupole magnets are conducted for the initial and maximum luminosity beam scenarios [18]. The corresponding beam and machine parameters are listed in Table 2. Twiss parameters and magnetic field values are listed in Table 3 and Table 4, respectively. .

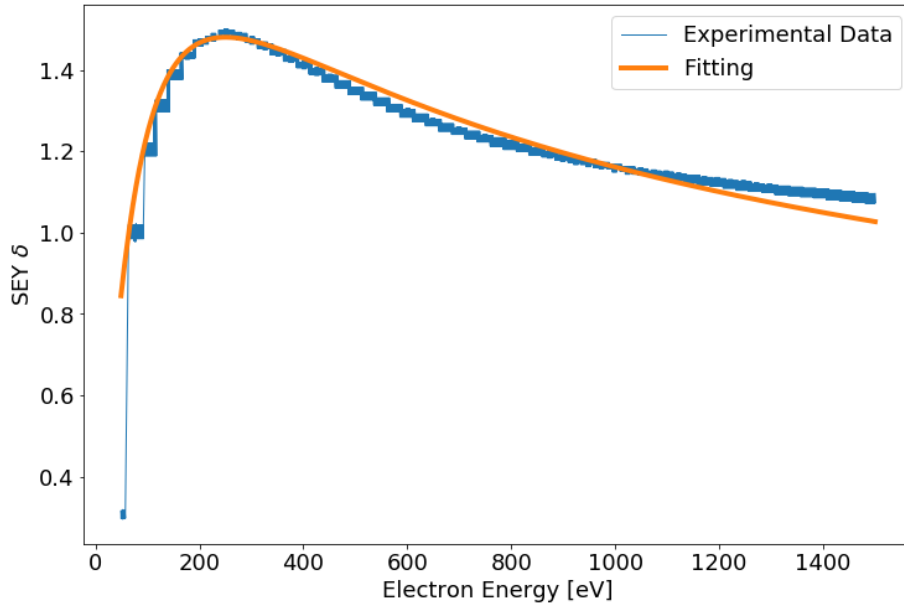


Fig. 15: Measured stainless steel SEY curve and fitting to the ECLLOUD model [19].

The existing RHIC vacuum chamber is made of the same material as the

Fermilab Main Injector and CERN SPS. The SEY of scrubbed stainless steel (SS316L) has been measured at the Fermilab Main Injection after scrubbing with a proton beam for several years [19]. Data fitted into the E-CLOUD model well. The beam-conditioned stainless steel SEY curve from CERN SPS [20] displays a similar δ_{max} . Table 1 lists the secondary emission parameters for stainless steel used in our simulations.

Table 2: Beam and machine parameters relevant to the EC simulations for the initial and the maximum luminosity beams of the EIC hadron storage ring

Parameter	Unit	Initial luminosity	Maximum luminosity
Particle energy	GeV	275	275
No. of bunches per beam		290	1160
No. of bunches in gap		25	100
Bunch population	10^{10}	10.2	6.9
RMS emittance (H,V)	nm	(17.9,8.5)	(9.2,1.6)
normalized RMS emittance (H,V)	μm	(5.25,2.5)	(2.7, 0.47)
average β^* in arc	m	25	25
RMS bunch size σ^* (H, V)	mm	(0.67, 0.46)	(0.48, 0.2)
RMS bunch length σ_l	cm	9.9	6
RMS energy spread	10^{-4}	4.6	6.8
Bunch space	ns	40.5	10.14
Radius of beam pipe	m	0.035	0.035

Table 3: Twiss parameters for dipole, quadrupole and sextupole magnets of the SC arcs of the EIC hadron storage ring (hCR-200429 lattice) and warm sections

Parameter	Unit	Dipole	Quadrupole	Sextupole	Warm
Betax	m	29.76	35.60	34.54	40
Betay	m	31.38	44.57	32.14	40
Dx	m	0.93	0.77	1.16	1.16

For the initial luminosity beam, the heat load deposited from the EC on the beam pipe of the dipole and quadrupole magnets is 0.78 W/m and 3.94 W/m, respectively. For the maximum luminosity beam, the values become 9.92 W/m and 27.26 W/m, close to or higher than 0.5 W/m, the available dynamic heat load budget to the 4.5 K stainless steel beam pipe. This means the existing

Table 4: Magnetic field values for the SC arc magnets of the EIC hadron storage ring (hCR-200429 lattice)

Magnet type	Unit	Strength	Gradient	Comments
Dipole	T	*	3.78	*
Quad-triplet	T/m	0.052	47.4	*
Quad-trim	T/m	0.024	22.0	*
Quad-main	T/m	0.092	84	Q4,Q5,Q6,Q7
Quad-kf/kd	T/m	0.085	72	arc quads
Sextuple-sd	T/m ²	0.72	658.3	near quads
Sextuple-sf	T/m ²	0.31	280	near quads

RHIC stainless steel beam pipe is not suitable for the EIC.

4.3. RHIC SC arc magnets with copper-coated beam pipe

To estimate whether a copper coating can have a low enough heat load for the EIC initial and maximum luminosity beams, the heat loads from EC have been computed for different SEY and depicted in Fig. 16. The SEY parameters of copper used for the simulations are shown in Table 1 and correspond to the default parameter values within the PyECLOUD code. Beam and machine parameters are listed in Table 5.

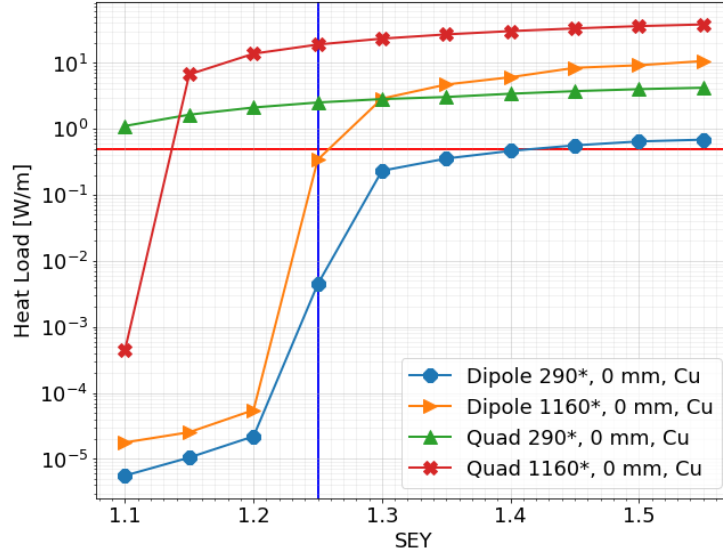


Fig. 16: Heat load as a function of SEY for the initial luminosity beam (290) and the maximum luminosity beam (1160) with a copper-coated beam pipe. The pressure of $1e-8$ Torr was used.

According to the LHC (copper) head load simulations, the SEY of about half of LHC cells is higher than 1.25 (even after LHC Run1 and Run2).

The vertical blue line in the plot represents a SEY of 1.25. The horizontal red line represents a heat load of 0.5 W/m. From Fig. 16, for a SEY of 1.25 and the maximum luminosity beam, the heat loads are 0.77 W/m and 19.26 W/m for the dipole and quadrupole, respectively, and 0.10 W/m and 2.54 W/m for the initial luminosity beam. Results are summarized in Table 5. Note that, for a quadrupole magnet beam pipe with SEY of 1.1, the higher heat load for the initial luminosity beam (with 290 bunches fill pattern or bunch spacing of 40 ns) than for the maximum luminosity beam (with 1160 bunches fill pattern or bunch spacing of 10 ns) can be explained by the discussion around Fig. 8.

Copper coating is not sufficient to resolve EC issues in the EIC hadron storage ring beam pipe. Therefore, in the next section, we explore the performance of

amorphous carbon coating, with SEY ~ 1 .

Table 5: Stainless (SEY = 1.48) and copper (SEY=1.25) heat load for the initial and the maximum luminosity parameters

Magnet type	Unit	Initial luminosity	Maximum luminosity
Stainless Dipole	W/m	0.78	9.92
Stainless Quadrupole	W/m	3.94	27.26
Copper Dipole	W/m	0.23	0.34
Copper Quadrupole	W/m	2.50	18.9

4.4. RHIC SC arc magnets with amorphous carbon coated beam pipe

We simulated the EC buildup in different magnets for the maximum luminosity beam with an amorphous carbon-coated round beam pipe. The secondary electron parameters of amorphous carbon in Table 1 used for these simulations are obtained from Ref. [22]. The heat load as a function of δ_{max} (SEY) for the warm section (W) and the dipole (D), quadrupole (Q), and sextupole (S) magnets in the arc are shown in Fig. 17. EC builds up in the arc quadrupole magnet for a SEY of 1.15. Therefore amorphous carbon coating with a SEY lower than 1.1 should be fine.

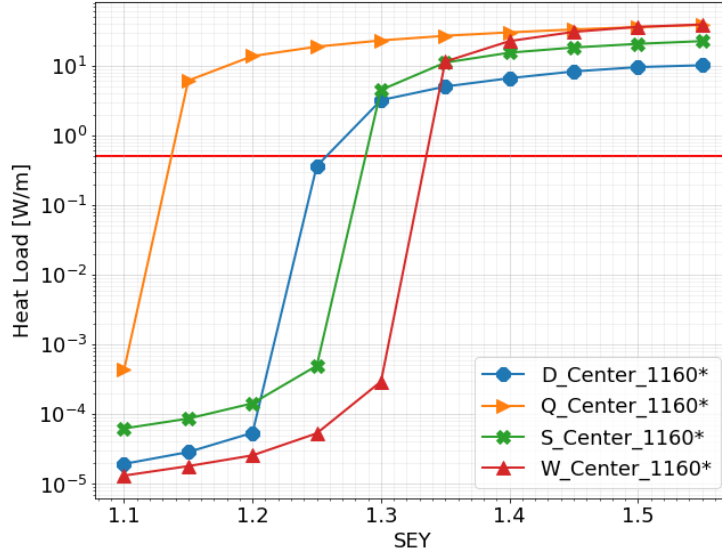


Fig. 17: Heat load with a-C coating for the maximum luminosity beam.

4.5. EC thresholds with horizontal beam offset

EIC is designed for a wide range of centers of mass energies [18]. To achieve electron-ion collision at IP6, the revolution frequency or circumference of the hadron beam will be changed to match the electron beam frequency. This requires a significant horizontal beam offset in the arcs of the EIC hadron ring.

A lattice with radial shift has been developed [23]. The required horizontal beam offsets at the arc dipole, quadrupole, and sextupole magnets are extracted from the lattice and shown in Fig. 18. The closed orbit is shown in Fig. 19. The mean orbit offset in an arc is about 12.5 mm. From Fig. 18 the maximum horizontal beam offset at the quadrupole and sextupole magnets is about 18 mm, while it is 14-16 mm at the dipole magnets. EC buildup with a horizontal beam offset is evaluated in this section.

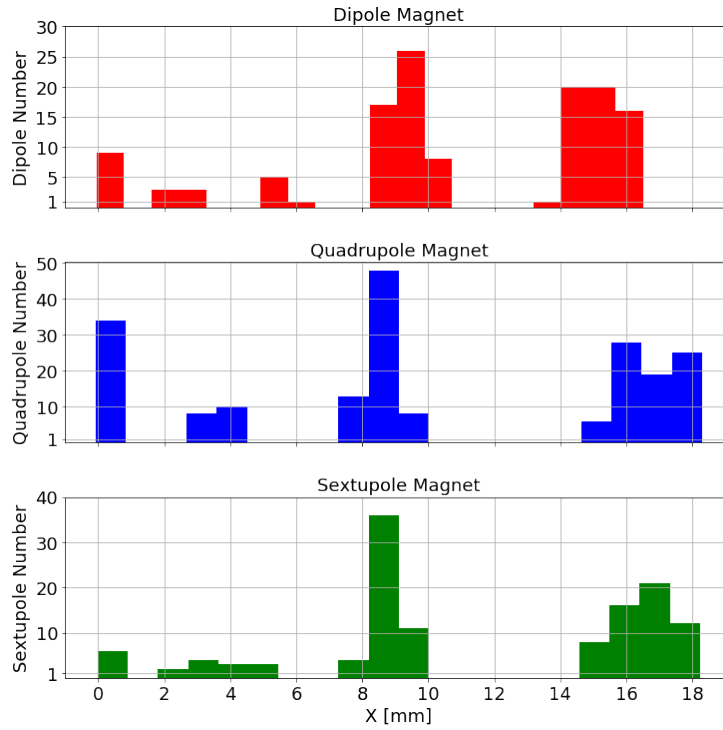


Fig. 18: Horizontal beam offset distribution at different arc magnets

For the initial luminosity beam (275 GeV beam of 290 bunches with 19.1×10^{10} protons per bunch) with a horizontal offset of 18 mm, the heat load curves for different magnets are shown in Fig. 20. According to the curve of the quadrupole magnet, one can find that the a-C should present a SEY lower than 1.15.

In the case of the maximum luminosity beam (275 GeV beam of 1160 bunches

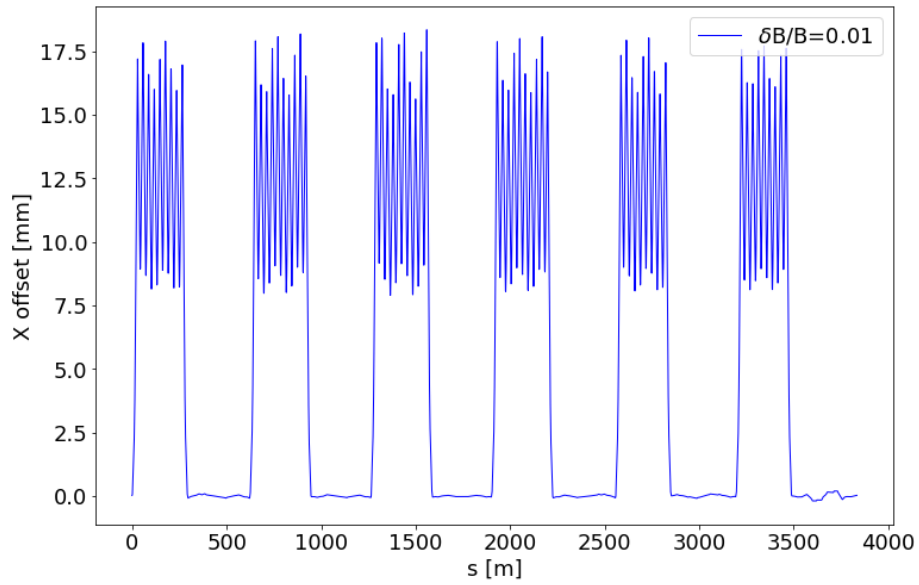


Fig. 19: Beam orbit with about 18 mm maximum horizontal beam offset.

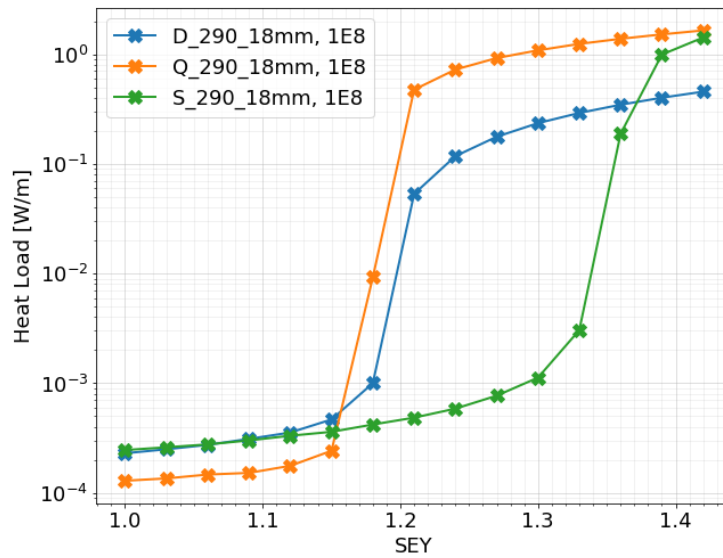


Fig. 20: Heat load with a-C coating for the initial luminosity beam (290 bunches fill pattern with 18 mm horizontal offset.)

with 6.9×10^{10} protons per bunch with 18 mm horizontal offset), as defined by the sextupole heat load curve, the maximum SEY should be less than 1.02. The

reason that the sextupole magnet shows the highest EC heat load delves on the discussion around Fig. 22. The secondary electron density for the sextupole magnet is about 2 orders higher than for the quadrupole magnet.

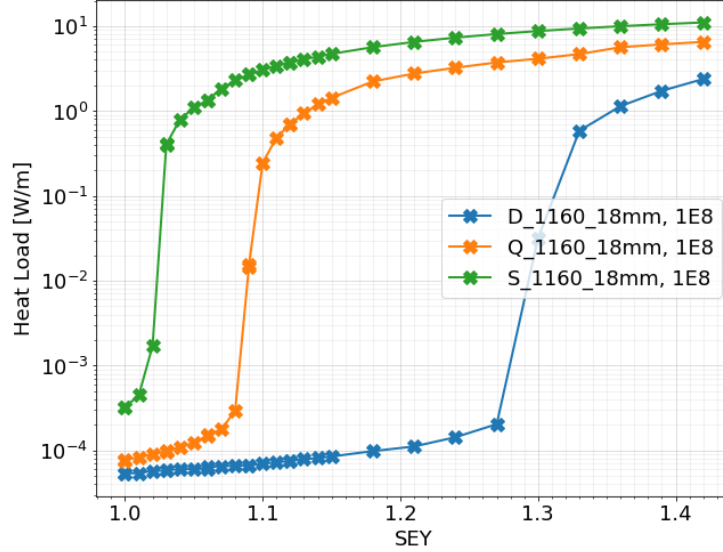


Fig. 21: Heat load with a-C coating for the maximum luminosity beam (1160 bunches fill pattern with 18 mm horizontal offset).

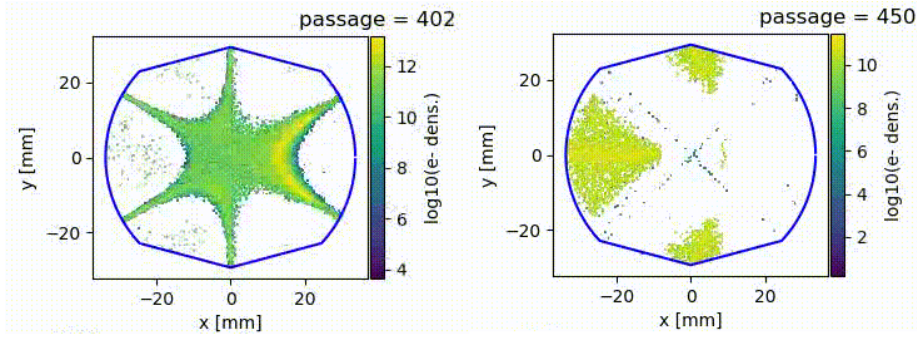


Fig. 22: Secondary electrons density for sextupole (left) and quadrupole (right) magnets with 1160 bunches fill pattern.

The heat loads for the arc quadrupole, sextupole, and dipole magnets and the warm sections are also scanned with different horizontal offsets. From Fig. 23, we can find that the heat loads for the sextupole and the quadrupole magnets are significantly affected by the horizontal offset.

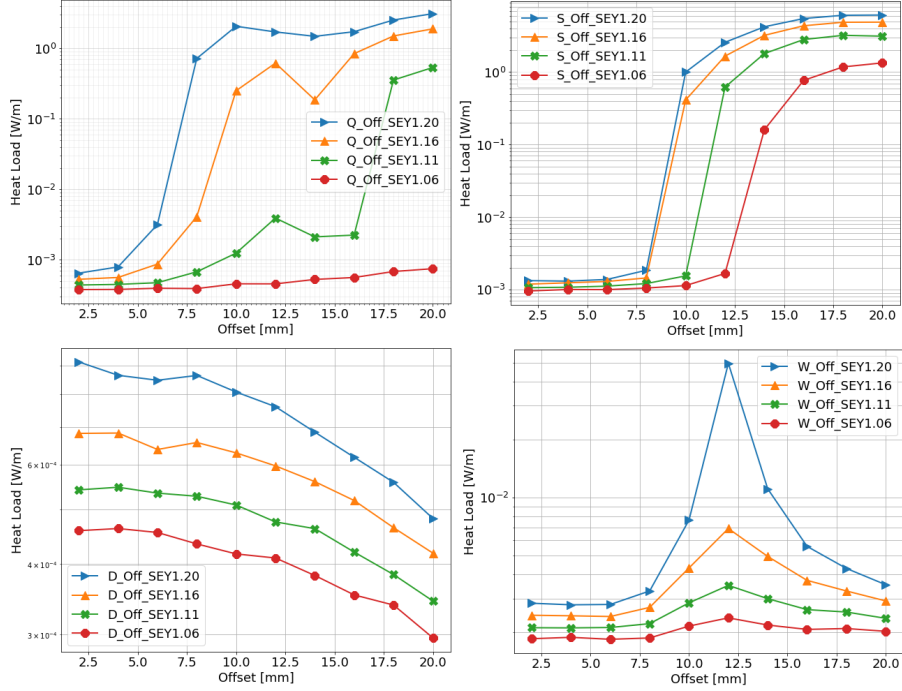


Fig. 23: Heat load for the arc quadrupole (top left), sextupole (top right), and dipole (bottom left) magnets and for the warm section (bottom right) with the 1160 bunches fill pattern.

4.6. EC thresholds for the warm region

To find the horizontal beam offset limit (tolerance) in the warm straight drift (no field) sections - currently equipped with NEG coating - we performed EC buildup simulations using the copper SEY parameters, because of the lack of the NEG SEY parameters. The corresponding beam and machine parameters are listed in Table 2. Twiss parameters and SEY values are listed in Table 3 and Table 1, respectively. The heat load from EC computed for different beam configurations is depicted in Fig. 24.

The horizontal beam offset should be kept below ~ 6 mm in a warm section/drift space with a NEG SEY of 1.25. Lower SEY values relax the horizontal beam offset limitation. NEG coating can show a SEY of less than 1.25 when vacuum-baked above 160 degrees Celsius for more than 2 hours.

4.7. EC thresholds for the Interaction Region (IR) vacuum chamber

The vacuum chamber in the EIC IR has a different radius (Fig. 25) with different magnet strengths and gradients (Table 6). Therefore, to check whether a-C coating is required or not, we did some EC buildup simulations for the IR region.

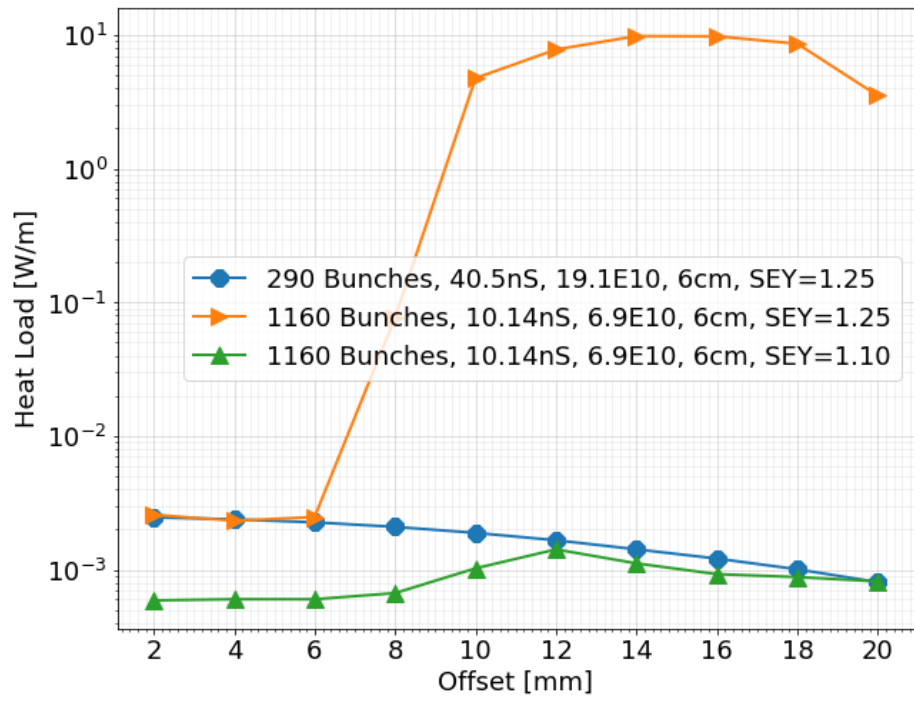


Fig. 24: Heat load for the warm section.

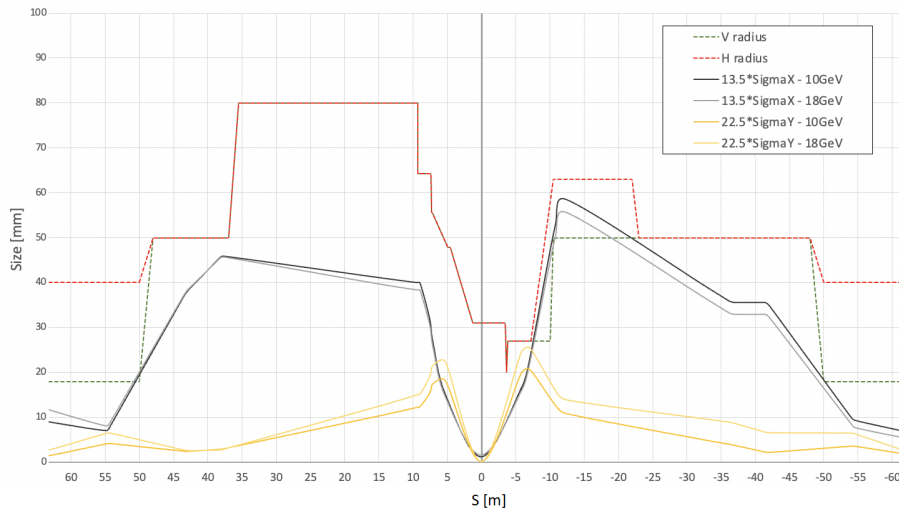


Fig. 25: Dimensions of the IR vacuum chamber.

Table 6: Magnetic field parameters in the IR region.

Magnet	Length[m]	IR1/IR2[cm]	Dipole Field[T]	Gradient[T/m]
B0pF	1.2	17	-1.3	0
B0ApF	0.6	4.3	3.3	0
B1pF	3	13.5	3.4	0
B1ApF	1.5	16.8	2.7	0
Q1ApF	1.46	5.6	0	-77.9
Q1BpF	1.61	7.8	0	-63
Q2pF	3.6	11.3	0	39.7
Q1ApR	1.8	2.0/2.52	0	78
Q1BpR	1.4	2.8	0	78
Q2pR	4.5	5.4	0	34

First, we did some EC buildup simulations for the quadrupole Q1ApR with 0 mm offset and 20 mm pipe radius, with copper and a-C coating respectively - heat load results are shown in Fig. 26). a-C coating is needed for that region. Secondly, we did some EC buildup simulations for the IR warm section with copper coating and different beam pipe radii - see Fig. 27 and Fig. 28.

These plots indicate that for the 1160 bunches beam, the heat loads from EC are high for a beam pipe radii close to 20 mm and 45 mm if the copper coating is used. For the 290 bunches beam, the heat loads are high for a beam pipe radii between 40 mm and 70 mm. Thus, a-C coating or NEG coating, or a 100 Gauss solenoid field) is needed for the IR warm region beam pipe with this radius. This conclusion is also valid for other warm regions (no field) which is discussed in the previous section.

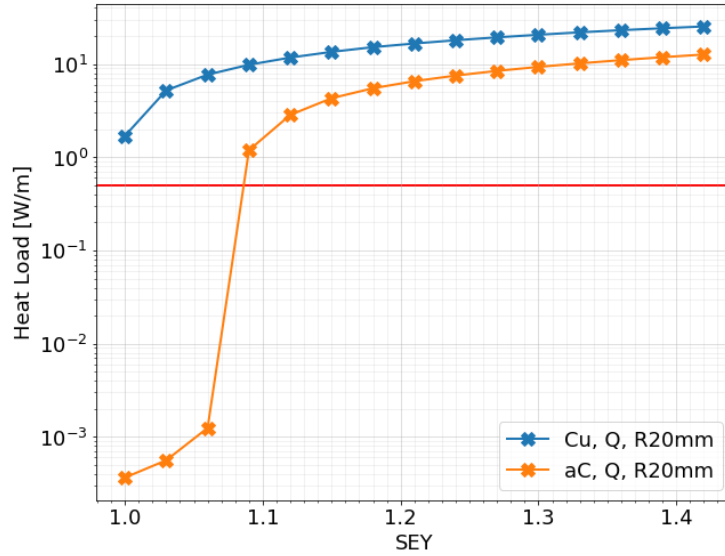


Fig. 26: Heat load for the quadrupole (Q1ApR: 0mm offset, 20 mm pipe radius) with copper and a-C coating.

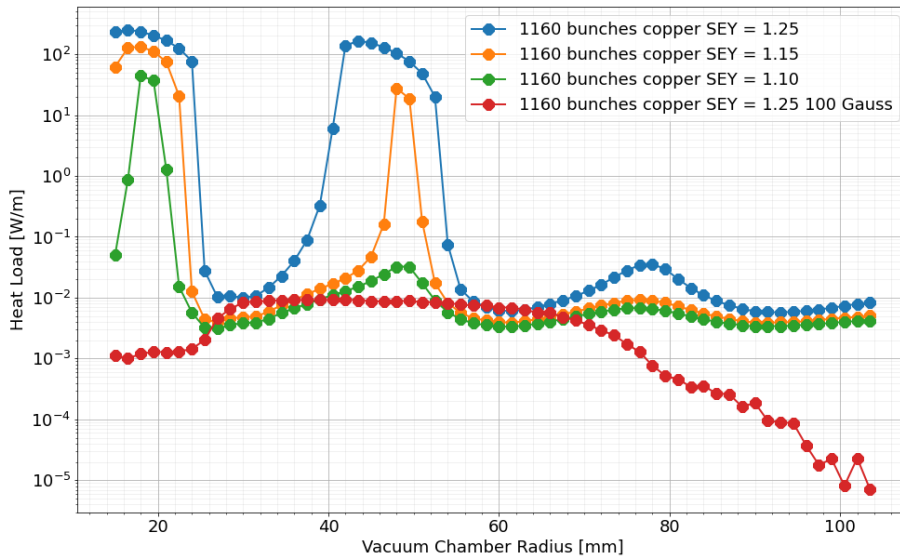


Fig. 27: 1160 Bunches: Heat load for the warm section with copper coating and different beam pipe radius.

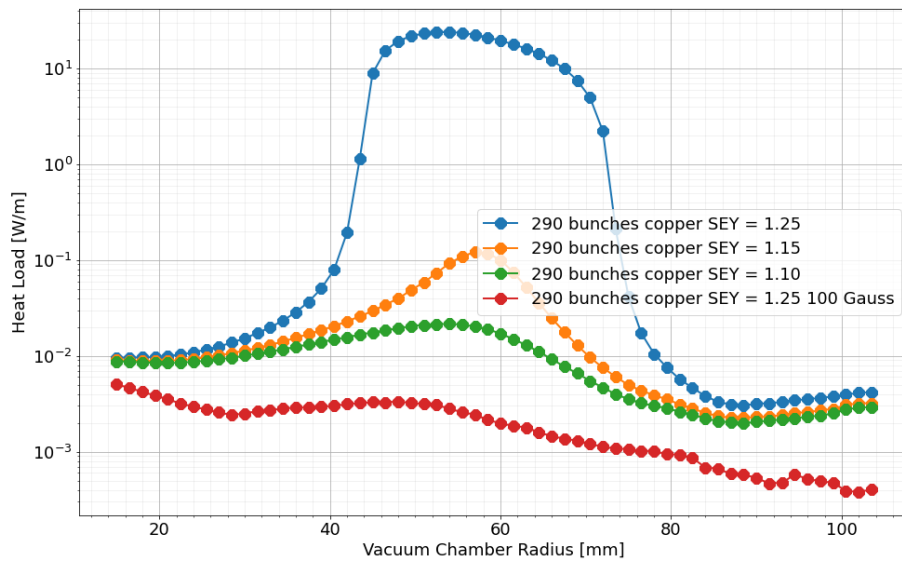


Fig. 28: 290 bunches: Heat load for the warm section with copper coating and different beam pipe radius.

5. Summary

Our studies show that a surface of amorphous carbon (a-C) can mitigate the EC buildup in the vacuum chamber of the EIC hadron storage ring arcs and a SEY lower than 1.02 is required at the arc sextupole magnets to suppress EC.

For the straight section with a 35 mm beam pipe radius, the horizontal beam offset has to be limited to less than 8 mm if the SEY of the beam pipe surface is 1.25. Lower values of SEY can be provided by NEG coating when activated above 160 degrees Celsius.

According to the preliminary EC simulations in the interaction region (IR), a-C coating is also suggested. Additional simulations for the different apertures with two beams in the interaction region may be needed. More simulations with different energy (injection energy, during transition or ramp), with different beta functions may be needed in the future.

At the interaction point (IP), the hadron beam will collide with the electron beam. The heat load with two beams will be evaluated as well with two different coating materials, copper and a-C.

6. Acknowledgments

The authors appreciate the help from Steve Peggs for providing the lattice twiss parameters and magnet strengths. We also would like to thank Giovanni Iadarola for his help with the PyECLLOUD code.

7. Appendix A: The Furman-Pivi Model

For the Furman-Pivi (FP) model, the SEY is expressed as three components:

$$\delta(E_0, \theta_0) = \delta_{elas}(E_0, \theta_0) + \delta_{true}(E_0, \theta_0) + \delta_{redif}(E_0, \theta_0) \quad (10)$$

In the FP model, the ‘re-diffused’ component $\delta_{redif}(E_0, \theta_0)$ is included. The re-diffused electrons are the electrons that emit out again from the surface after losing some energy in the material. The elastic component $\delta_{elas}(E_0, \theta_0)$ is a function of both energy and angle while in the ECLLOUD model it is the only function of the energy.

The three components use the following expressions:

$$\delta_{elas}(E_0, \theta_0) = \delta_{elas}(E_0)[1 + e_1(1 - \cos^{e_2}\theta_0)] \quad (11)$$

$$\delta_{redif}(E_0, \theta_0) = \delta_{redif}(E_0)[1 + r_1(1 - \cos^{r_2}\theta_0)] \quad (12)$$

$$\delta_{true}(E_0, \theta_0) = \delta_{max}(\theta_0) \frac{s \frac{E_0}{E_{max}(\theta_0)}}{s - 1 + (\frac{E_0}{E_{max}(\theta_0)})^s} \quad (13)$$

While $\delta_{elas}(E_0)$, $\delta_{redif}(E_0)$, $\delta_{max}(\theta_0)$ and $E_{max}(\theta_0)$ in above equations are ex-

pressed as below:

$$\delta_{elas}(E_0) = P_{1,e}(\infty) + [\hat{P}_{1,e} - P_{1,e}(\infty)]e^{-(|E_0 - \hat{E}_e|/W)^p/p} \quad (14)$$

$$\delta_{redif}(E_0) = P_{1,r}(\infty)[1 - e^{-(E_0/E_r)^r}] \quad (15)$$

$$\delta_{max}(\theta_0) = \delta_{max}[1 + t_1(1 - \cos^2 \theta_0)] \quad (16)$$

$$E_{max}(\theta_0) = E_{max}[1 + t_3(1 - \cos^4 \theta_0)] \quad (17)$$

where $e_1, e_2, r_1, r_2, P_{1,e}(\infty), P_{1,r}(\infty), \hat{P}_{1,e}, \hat{E}_e, E_r, W, p, r, t_1, t_2, t_3$ and t_4 are FP model parameters which should be obtained via fitting SEY experimental data. The SEY curves of the FP model and their angle dependencies are plotted in Fig. 29 and Fig. 30.

The energy distribution or spectrum ($0 \leq E \leq E_0$) for these three kinds of secondary electrons are listed below:

$$f_{1,elas} = \frac{2e^{-(E-E_0)^2/2\sigma_{elas}^2}}{\sigma_{elas}\sqrt{2\pi}erf(E_0/\sigma_{elas}\sqrt{2})} \quad (18)$$

$$f_{1,redif} = \frac{q+1}{E_0^{q+1}}E^q \quad (19)$$

$$f_{n,true} = A_n E^{P_n-1} e^{-E/\epsilon_n} \quad (20)$$

where $\sigma_{elas}, q, p_n, A_n$ and ϵ_n are all model parameters. In the PyECLoud code, σ_{elas} has been modified to $\sigma_{elas} = \sigma_{elas} - 1.88 + 2.5[1 + \tanh(0.01(E_0 - 150))]$.

Fig. 31, Fig. 32 and Fig. 33 depict the energy distribution for different incident energy electrons. In the FP model, the emitted electron energy distribution depends on different component types, incident energy E_0 and n . n is the number of true secondary in the FP model.

The FP model also uses the cosine distribution for all three kinds of emitted electrons. This is different from the ECLoud model which only applies the cosine angular dependence to the true secondary electrons (Eq.3). In the ECLoud model, there are only elastically reflected electrons and true secondary electrons. There is no re-diffused electron component since the separation between the re-diffused electrons and the true secondary electrons become arbitrary [12].

References

- [1] A. Romano et al., Electron cloud buildup driving spontaneous vertical instabilities of stored beams in the Large Hadron Collider. PRAB 21, 061002 (2018):<https://journals.aps.org/prab/pdf/10.1103/PhysRevAccelBeams.21.061002>
- [2] G. Arduini et al., High Luminosity LHC: challenges and plans. JINST 11 C12081 (2016): <https://iopscience.iop.org/article/10.1088/1748-0221/11/12/C12081/pdf>

- [3] K. Brodzinski and L. Tavian, First measurements of beam-induced heating on the LHC cryogenic system, Report No. CERN-ATS-2013-009 (CERN, Geneva, Switzerland, 2013); in International Cryogenic Engineering Conference/ International Cryogenic Materials Conference, Fukuoka, Japan, May 2012 (Cryogenics and Superconductivity Society of Japan, Tokya, 2012).
- [4] T. Abe et al., Achievements of KEKB. Prog. Theor. Exp. Phys. 2013, 03A001 (2013): <https://academic.oup.com/ptep/article/2013/3/03A001/1556871>
- [5] Y. Funakoshi, KEKB Accelerator Physics Report: <https://www.classe.cornell.edu/public/icfa/proceedings/pdf/yfunakoshi2.pdf>
- [6] Y. Suetsugu, K.-I. Kanazawa, K. Shibata, T. Ishibashi, H. Hisamatsu, M. Shirai, and S. Terui, Design and construction of the SuperKEKB vacuum system, J. Vac. Sci. Technol. A 30, 031602 (2012).
- [7] J. A. Crittenden, J. Conway, G. F. Dugan, M. A. Palmer, D. L. Rubin, J. Shanks, K. G. Sonnad, L. Boon, K. Harkay, T. Ishibashi, M. A. Furman, S. Guiducci, M. T. F. Pivi, and L. Wang, Investigation into EC effects in the International Linear Collider positron damping ring, Phys. Rev. ST Accel. Beams 17, 031002 (2014).
- [8] R. Than, S. Verdú-Andrés, S. Berg *et al.*, High current, high-temperature operation test of the superconducting magnets in the RHIC yellow ring, EIC Technical Note EIC-ADD-TN-020, Brookhaven National Lab, Upton, NY (2021): <https://www.osti.gov/servlets/purl/1822339>
- [9] <https://github.com/PyCOMPLETE/PyECLLOUD>
- [10] Giovanni Iadarola, CERN-THESIS-2014-047.
- [11] M. A. Furman and M. T. F. Pivi. Probabilistic model for the simulation of secondary
- [12] R. Cimino, I. R. Collins, M. A. Furman, M. Pivi, F. Ruggiero, G. Rumolo, and F. Zimmermann Phys. Rev. Lett. 93, 014801 Published 29 June 2004
- [13] CERN-ACC-2019-0029
- [14] The Furman Pivi model in PyECLLOUD, Theory, code implementation and simulation results
- [15] The correct and incorrect generation of a cosine distribution of scattered particles for Monte-Carlo modelling of vacuum systems Phys. Rev. ST Accel. Beams, 5:124404, Dec 2002.

- [16] Francis F. Chen, Introduction to Plasma Physics (1974)
- [17] Loizos Bitsikokos, Impact of the Secondary Emission Model on e-cloud build-up
- [18] eRHIC Preliminary Conceptual Design Report (2019)
- [19] Yichen Ji, Linda Spentzouris, SECONDARY ELECTRON YIELD MEASUREMENT AND EC SIMULATION AT FERMILAB, Proceedings of IPAC2015, Richmond, VA, USA MOPMA039.
- [20] Valentine Petit, In situ SEY measurements at the SPS. CERN Electron Cloud Meeting 63, Nov. 30, 2018.
- [21] Galina Skripka, Update on LHC arc heat load studies
- [22] <http://accelconf.web.cern.ch/ipac2016/doi/JACoW-IPAC2016-THPMY007.html>
- [23] EIC Technical Note, Number:EIC-ADD-TN-006

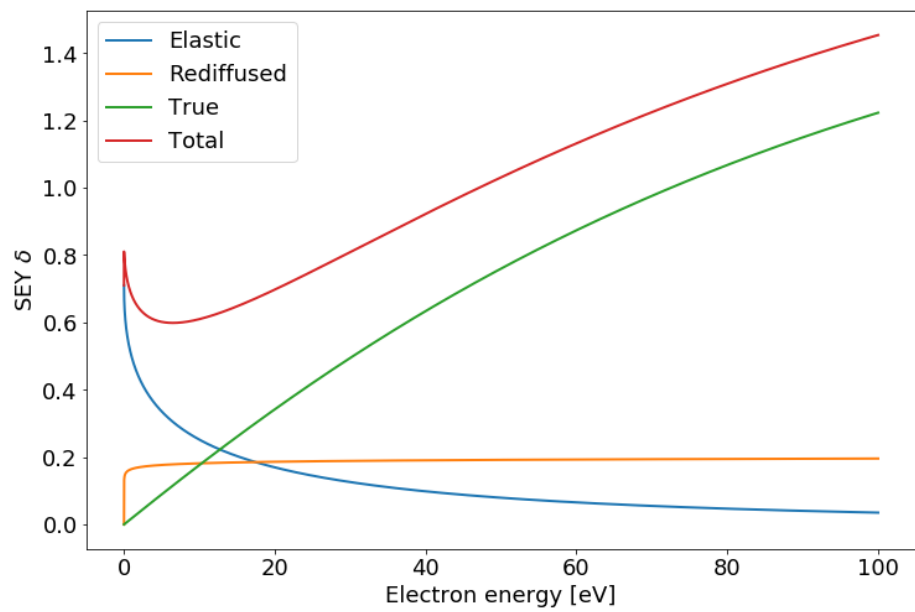
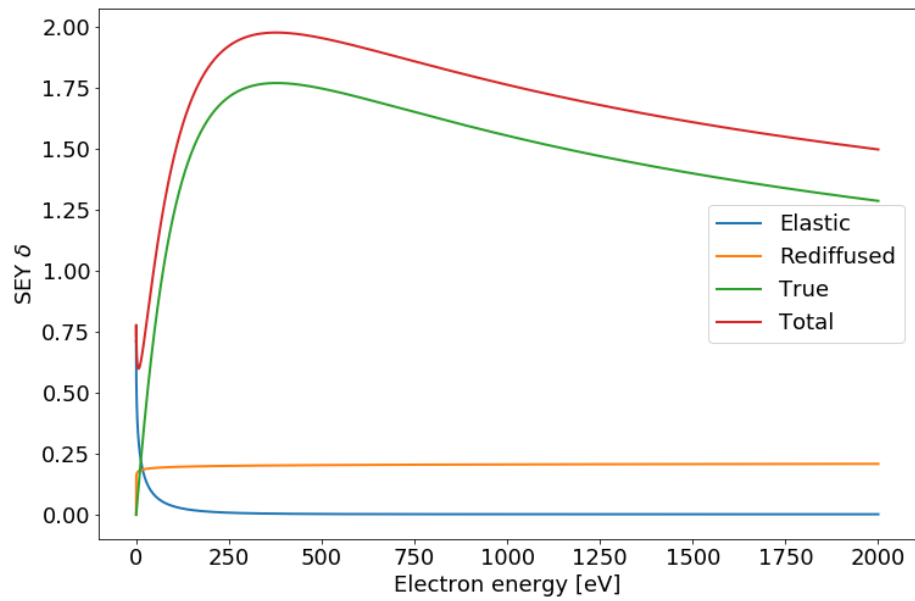


Fig. 29: SEY components for the FP model. Top: high incident energy. Bottom: low incident energy.

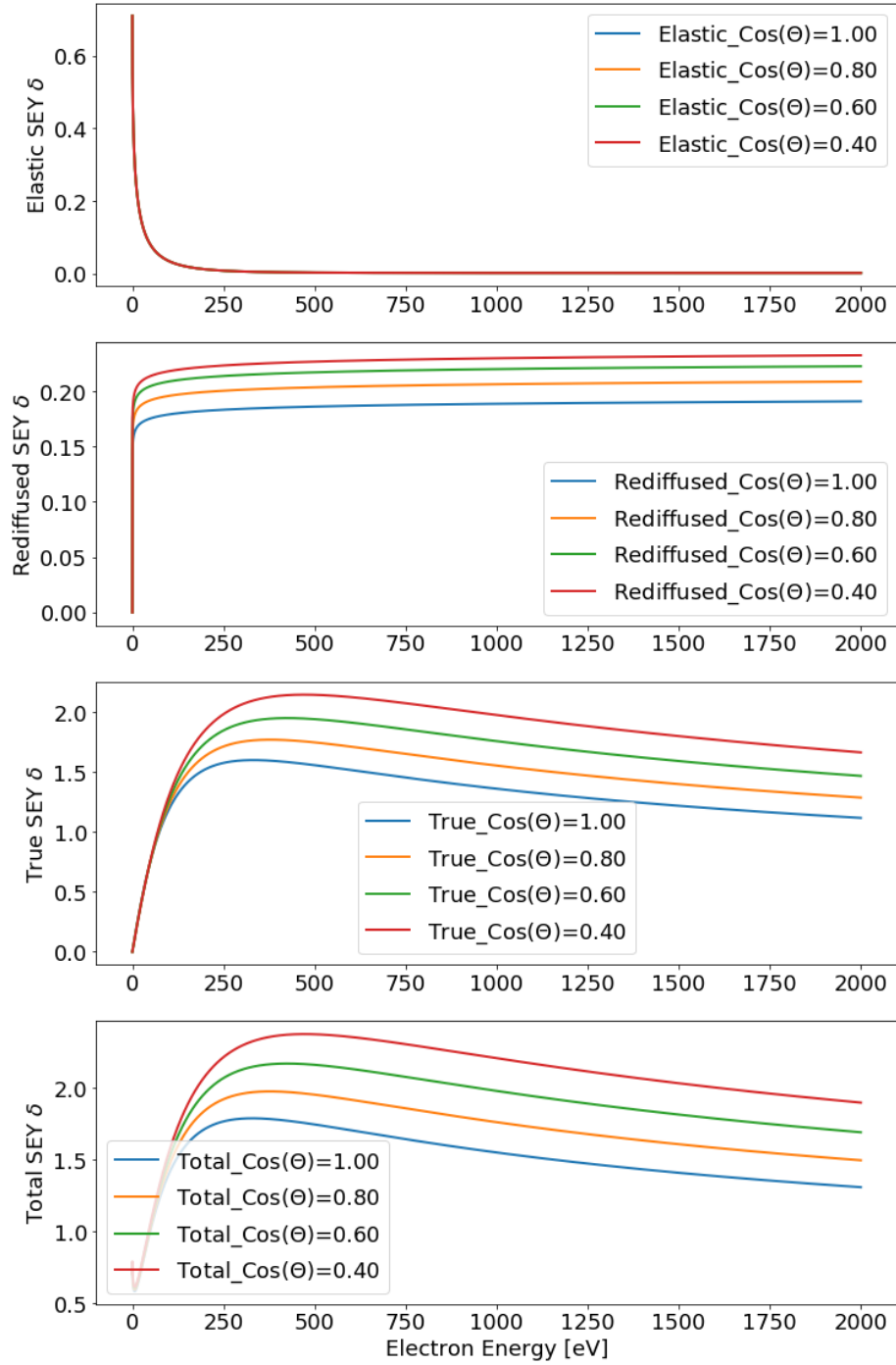


Fig. 30: SEY of FP model and its dependency on the incident angle. E_{max} and δ_{max} increase with the incident angle as for the ECLLOUD model.

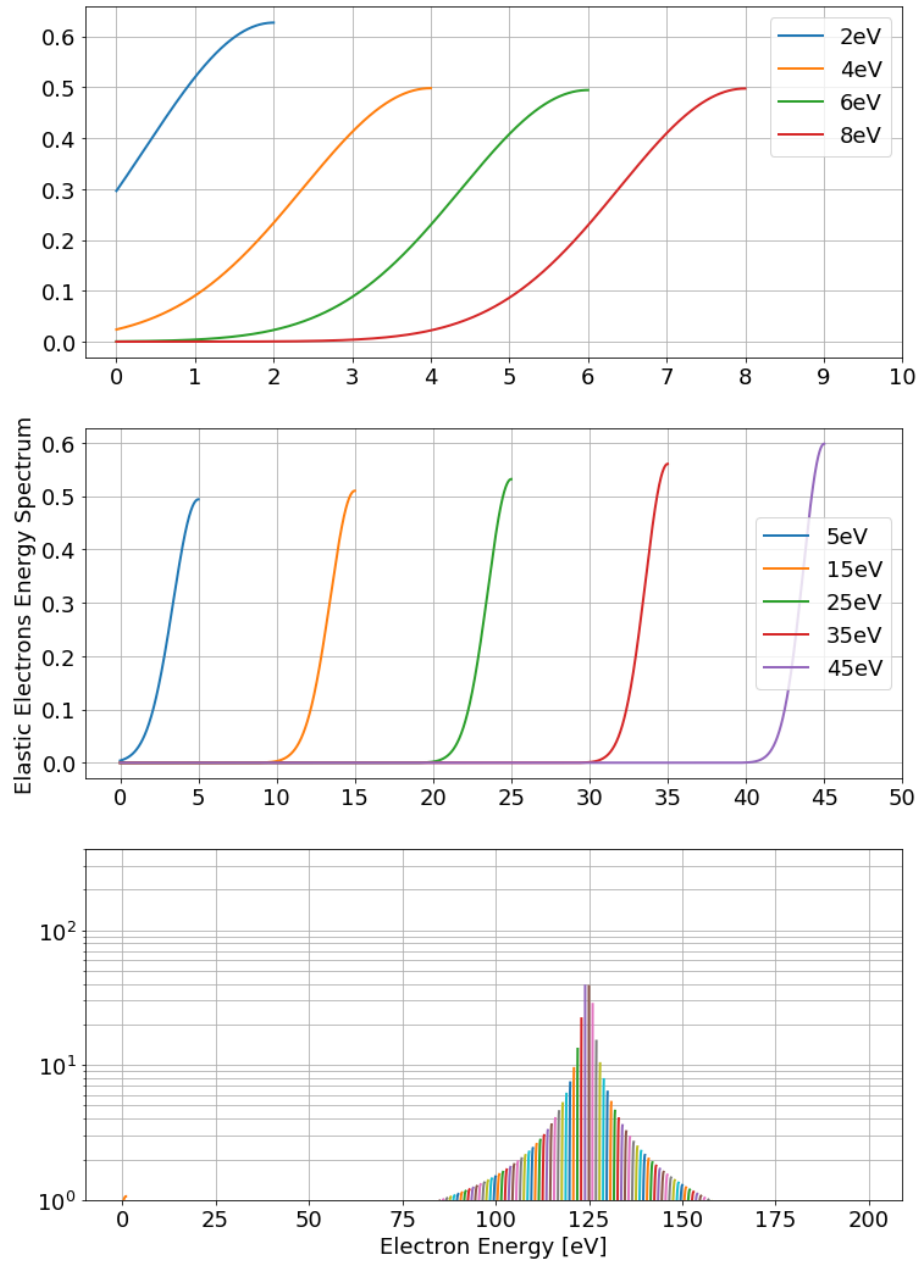


Fig. 31: The elastic electron spectrum of the FP model depends on the incident electron energy E_0 . Each line in this plot represents emitted electron spectrum computed for a fixed incident energy. The top, middle and bottom plots provide different energy ranges of incident electrons. ('use_modified_sigmaE' = True and 'SigmaE' = 1E-4)

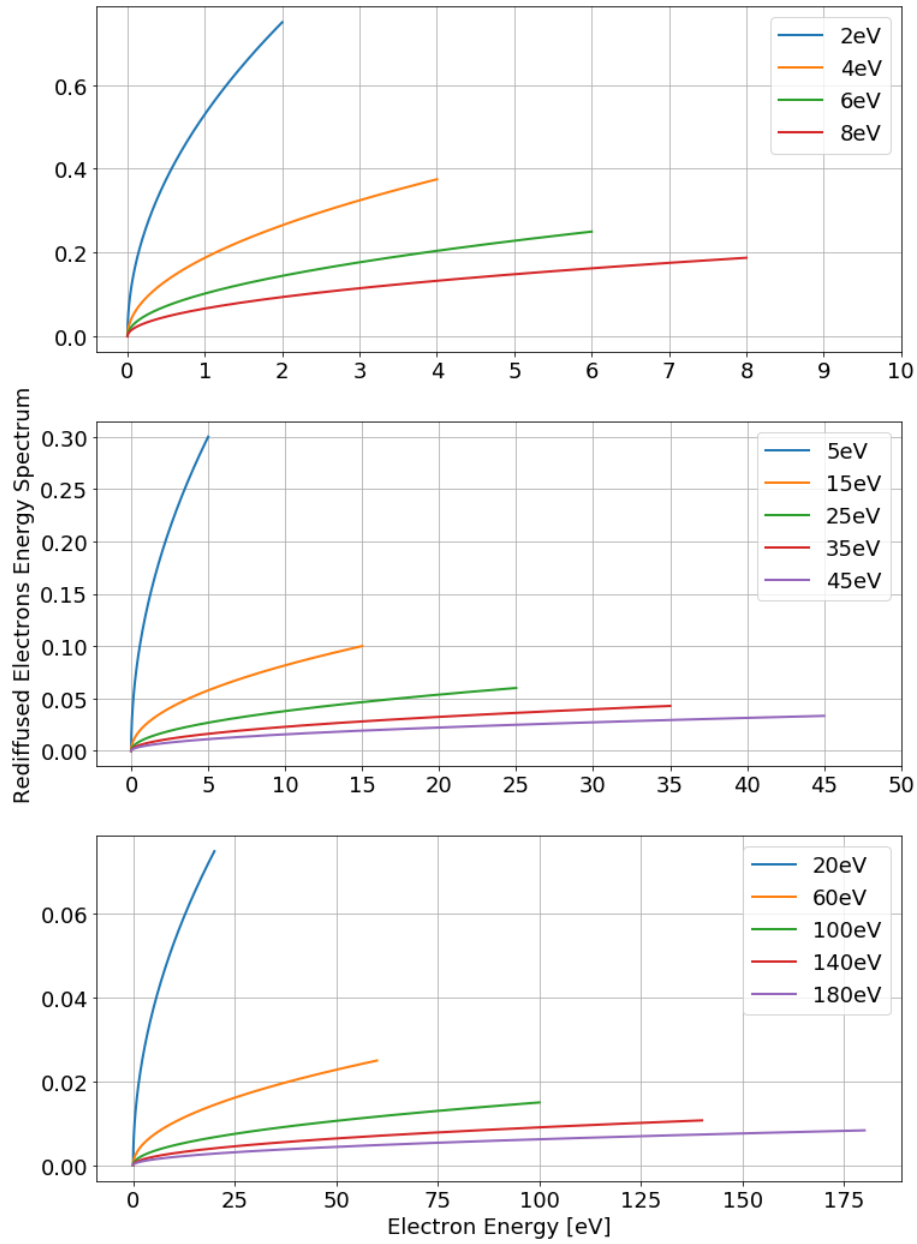


Fig. 32: The rediffused electron spectrum of the FP model depends on the incident electron energy E_0 . Each line in this plot represents the rediffused electron spectrum computed for a fixed incident energy. The top, middle and bottom plots provide different energy ranges of incident electrons.

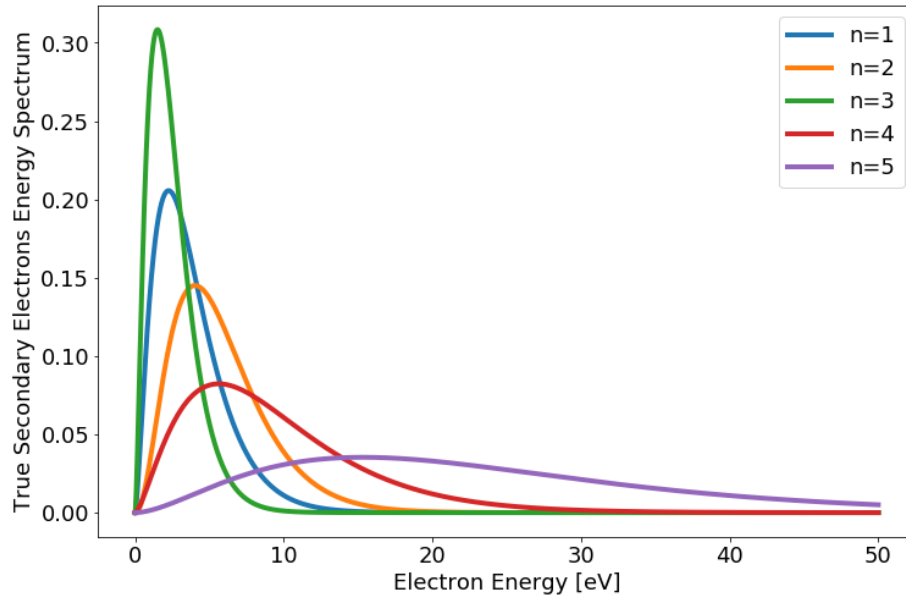


Fig. 33: The true secondary electron spectrum of the FP model depends on n , the number of emitted true secondary electrons.

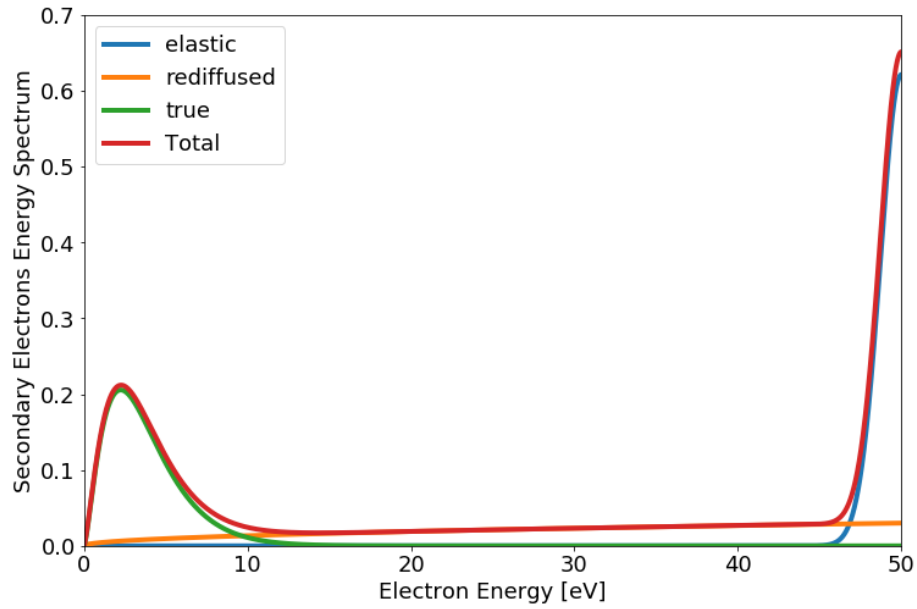


Fig. 34: Secondary electron spectra of the FP model for 50 eV incident electrons. $n = 1$ is used here.

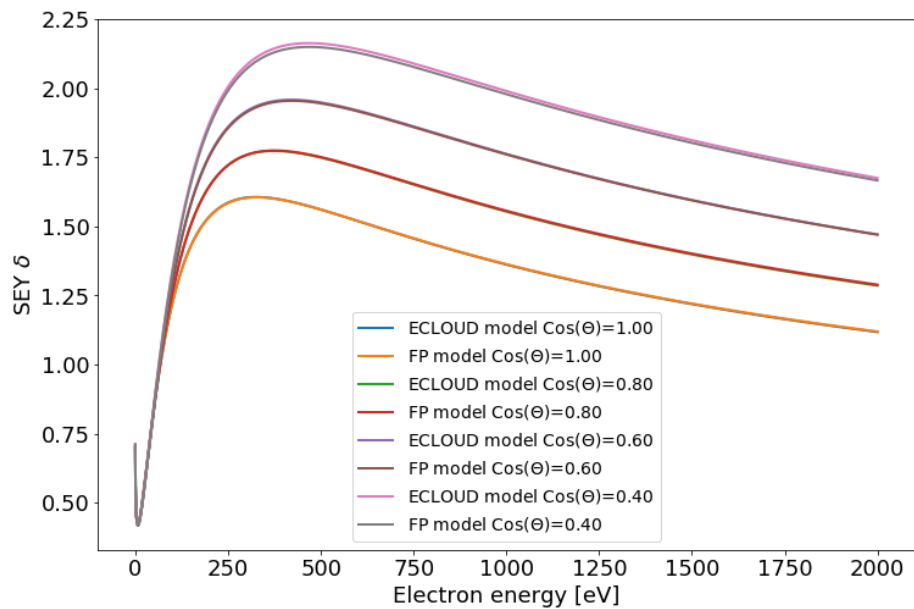


Fig. 35: SEY curves for ECLLOUD and FP model.

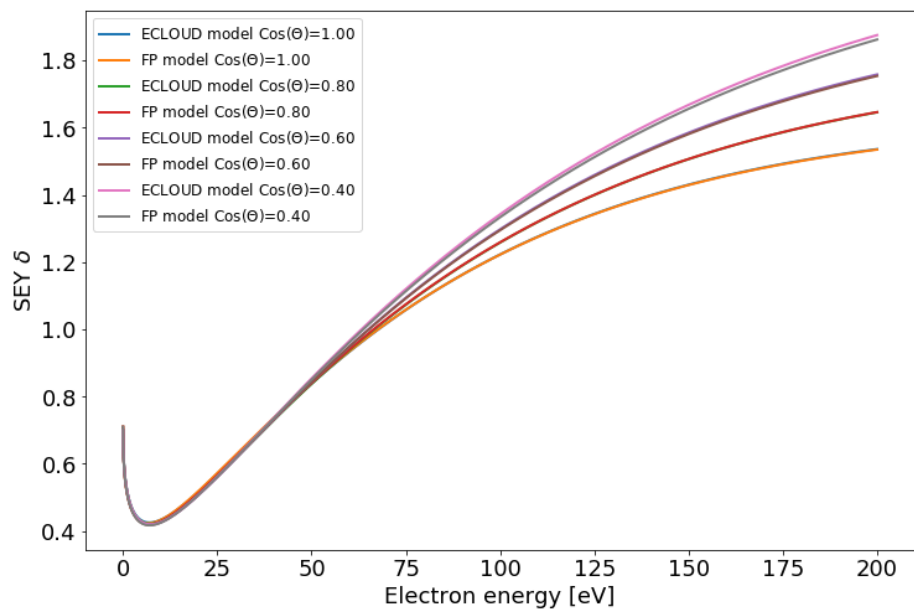


Fig. 36: SEY curves for ECLLOUD and FP model (low incident energy).